metals

Article

Mechanical Response and Failure Evolution of 304L Stainless Steel under the Combined Action of Mechanical Loading and Laser Heating

Mohsan Jelani [1], Zewen Li [2,*], Zhonghua Shen [1,2], Najam Ul Hassan [3] and Maryam Sardar [1]

1 School of Science, Nanjing University of Science and Technology, Nanjing 210094, China; jelani373@gmail.com (M.J.); shenzh@njust.edu.cn (Z.S.); maryam.ac.cn@gmail.com (M.S.)
2 Advanced Launching Co-innovation Centre, Nanjing University of Science and Technology, Nanjing 210094, China
3 School of Materials Science and Engineering, Nanjing University of Science and Technology, Nanjing 210094, China; najamphys@gmail.com
* Correspondence: lizewen@njust.edu.cn; Tel.: +86-25-8431-5687

Received: 15 June 2018; Accepted: 2 August 2018; Published: 7 August 2018

Abstract: Deformation and fracture properties of structural materials are greatly influenced by the factors like applied load, state of stress, and temperature. A precise prediction of the material properties of stainless steel at elevated temperature is necessary for determining the load-carrying capacity of structures under severe conditions. The present work reports the deformation and failure characteristics of 304L stainless steel subjected to combined laser heating and mechanical loading. The effect of main parameters on stress-strain, fracture characteristics, failure time, and temperature profile of specimens have been explored. Specimens were subjected to prescribed loading states, and then irradiated by a continuous wave fiber (1.08 μm) laser. The stress-strain curves indicated that the specimens experienced slight strain hardening in a specific temperature range prior to fracture. The specimen's ultimate failure time is found to be reduced by increasing either laser power density or preload level. Fracture on a microscopic scale was predominantly ductile, comprising dimples as well as micro-void nucleation, growth, and coalescence. With the increase of laser power density, dimples rupture is the primary fracture mode, while with the increase of preload value, relatively more in-depth and severe deformation effects were observed. The description and characterization of 304L stainless steel failure under the simultaneous action of laser heating and tensile stress have been explored in detail.

Keywords: 304L stainless steel; laser heating; tensile load; failure evolution; thermomechanical effects

1. Introduction

It is well known that the deformation and fracture properties of structural steels are significantly influenced by the factors like type of load, loading rate, and temperature [1,2]. Typically, 304L stainless steel is extensively used in a wide range of load-bearing applications due to its superior corrosion resistance, formability, and mechanical properties [1,3–5]. In structural engineering, different components may experience the severe thermal loading situations that might be induced by local intense fire, laser irradiation, or by aerodynamic heating [6]. The development of thermal stresses, along with a distinct degradation of mechanical properties at high temperatures, may considerably increase the possibility of fracture in structural components exposed to high operational loads [7,8]. It is therefore worthwhile to investigate the predictions of the mechanical responses of steel structures exposed to loaded conditions. An understanding of the plastic response of the 304L stainless steel under severe environment is crucial to develop a complete characterization of the material.

The variation in material strength with applied stress or strain is the key consideration in the design of classes of materials used in structures exposed to suddenly applied loads. Normally, materials dynamic deformation and failure mode are heavily dependent on the nature of stress, strain rate, and elevated temperatures [9–11]. With the tremendous development and access to high power laser systems, there is an emerging desire to understand the behavior of structural components under laser irradiation. Considering the laser damage effect of structural materials under severe situations, a brief review of related studies is presented. Yang et al. [12] explored Continuous Wave (CW) laser damage effect on steel structure under preloaded invariable stretching stress conditions. The dumbbell-shaped 30CrMnSiA steel sample was preloaded with invariable stretching force, and then irradiated by YAG laser. To relate the stretching stress and failure temperature, an empirical formula was proposed. Long et al. [13] established the relationships among different experimental factors including pre-load, laser power density, and the thickness on the rupture time of the composite laminates. Chang et al. [14] proposed an analytical tool for prediction of the behavior of composite and metallic structures exposed to simultaneous mechanical loading and intense laser heating. The developed methodology consists of a thermal analysis that describes nonlinear events like temperature dependent thermophysical parameters, re-irradiation losses, and melting or ablation processes. Medford et al. [4] developed a numerical model to predict fracture threshold and the thermomechanical response of structural materials under the conditions of simultaneous action of mechanical loading and laser heating. A remarkable reduction in room temperature tensile strength and damaging threshold energy was reported under the combined action of mechanical loading and laser exposure. Griffis et al. [7] experimentally determined the response of aluminum alloy subjected to simultaneous constant tensile load and rapidly localized heating condition. With the help of the developed thermal and stress computational model, the prediction of the required heating time for a ductile fracture of the irradiated section was obtained.

Considering laser heating of the preloaded materials, materials strength dependency on high temperature and strain rate is found to be complex and nonlinear. Due to the associated complexities in the laser heating (non-uniformity in temperature profile etc.) and dependency of material strength on strain and temperature, understanding how the structural components deform under transient impact conditions is still an open research field. The current work reported the effects of thermomechanical parameters on the deformation behavior and fracture characteristics of 304L stainless steel subjected to the simultaneous action of tensile loading and laser irradiations. A CW ytterbium fiber laser with a wavelength of 1.08 μm was employed to irradiate the specimens, while sample pre-loading was provided by the universal tensile testing machine. The stress-strain characteristics, stress relaxation behavior, failure time, temperature profiles, and fractographs have been explored in detail to characterize the 304L stainless steel failure mechanisms.

2. Materials and Methods

The material under investigation is 304L stainless steel supplied by ASM Inc. (Orlando, FL, USA) in the 2mm thick sheet form. Chemical composition (wt. %) of the 304L stainless steel reported from the supplier is 0.0237 C, 1.46 Mn, 0.299 Si, 17.99 Cr, 9.78 Ni, 0.022 Cu, 0.261 Mo, 1.191 Co and Fe to balance. The thermophysical and mechanical properties of the 304L steel are given in Table 1.

Table 1. Thermo-physical and mechanical properties of 304L stainless steel, data from [15,16].

Property	Value
Yield strength (MPa)	511
Density (g·cm^{-3})	7.9
Melting point (°C)	1410–1496
Absorption coefficient	0.30
Thermal conductivity (W·m^{-1}·K^{-1})	27

For the experimentation, test specimens were prepared into a rectangular, bar shape, with dimensions of 150 × 10 mm^2. The specimens were prepared with sufficient length (80 mm gauge length) to ensure a region about the center in which the temperature does not vary much along the length. Moreover, in normal tensile testing, the standard test sample (machined into a reduced section or in dog bone shape) is required to avoid fractures in the grips. In the present situation, since the gripped portion of the test specimen (heated by laser) is much cooler than the central part, a dogbone shape is not required to avoid fractures in the gripped section. Figure 1 provides a schematic presentation of laser irradiation to the preloaded specimen. The equipment arrangement for the experimental setup is available in the previously published article [17].

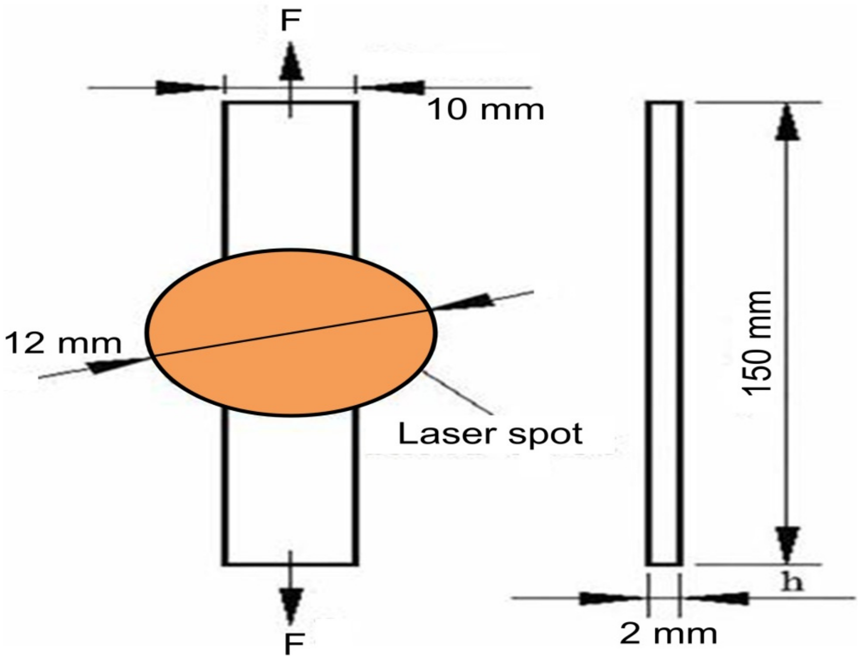

Figure 1. Schematic presentation of laser irradiation to the preloaded specimen.

Room temperature yield strength of the 304L stainless steel was measured using the universal tensile testing machine (JVJ-50S, SIOMM, Shanghai, China); average yield strength was found to be of 511 MPa. Experiments were performed under the conditions of four different preload levels, including 40%, 55%, 70%, and 85% of the measured yield strength (511 MPa) of 304L stainless steel. The actual values of preload levels are presented in Table 2. All the tensile loading tests were conducted using the above-mentioned universal tensile testing machine under a fixed crosshead speed of 3 mm/min. After reaching the prescribed load level, the specimens were kept under a constant loading state for a while before the laser was started. The loading profiles in the following Figures 3 and 4 represent the mechanical responses of the material after reaching the prescribed loading level (and the laser on), by ignoring the initial part (before reaching the prescribed load) of the loading curves.

Table 2. Experimental parameters: laser power densities and tensile load values.

Laser Power Density (W·cm^{-2})	398	556	696	883	972	1078
Stress (MPa)	205	281	358	434	...	...

The continuous wave ytterbium fiber laser (RFL-C1000, Raycus, Wuhan, China), with 1.08 μm wavelength and 1 kW maximum power output, was employed to heat specimens during the experiments. The laser started to irradiate the specimens after they reached a prescribed loading state. The distance between the laser emitter and the tensile loaded specimen was 70 cm. The laser spot with a 12 mm diameter was perpendicularly focused on the center of the test specimen. The laser spot size irradiating on the specimen was controlled by adjusting the distance from the focus lens to the specimen's surface. The experiments were conducted by employing a wide range of laser power densities, including 398 W·cm^{-2}, 556 W·cm^{-2}, 696 W·cm^{-2}, 883 W·cm^{-2}, 972 W·cm^{-2}, and 1078 W·cm^{-2} for each preload level. The specimens were continuously irradiated until their failure occurred and applied tensile load dropped to zero. To get more reliable results, the experiments were repeated three times under each condition. However, no considerable difference in the results of multiple trials was found.

During the experiment, the specimen fracture process was observed and recorded simultaneously with a high-speed video camera. An infrared radiation pyrometer (KMGA740-LO, Kleiber Infrared GmbH, Unterwellenborn, Germany) was used to record the temperature profile during the laser irradiation process. The temperature was recorded for the laser spot center at the front surface of the specimen which was directly exposed to laser irradiations. The tensile loading data was used to characterize the material strength degradation and stress/strain failure behavior. After the experiments, metallographic observations were conducted using a Scanning Electron Microscope (SEM, FEI Quanta 250F, Thermo Fisher Scientific, Hillsboro, OR, USA), in order to get a more in-depth analysis of the failure mode, and to understand the mechanism within the specimen's thickness.

3. Results and Discussions

3.1. Temperature Distribution

Temperature evolution of the spot center during laser irradiation for a wide range of laser power densities and preloads is illustrated in Figure 2. The exposed surface temperature increased sharply in the initial stage of interaction.

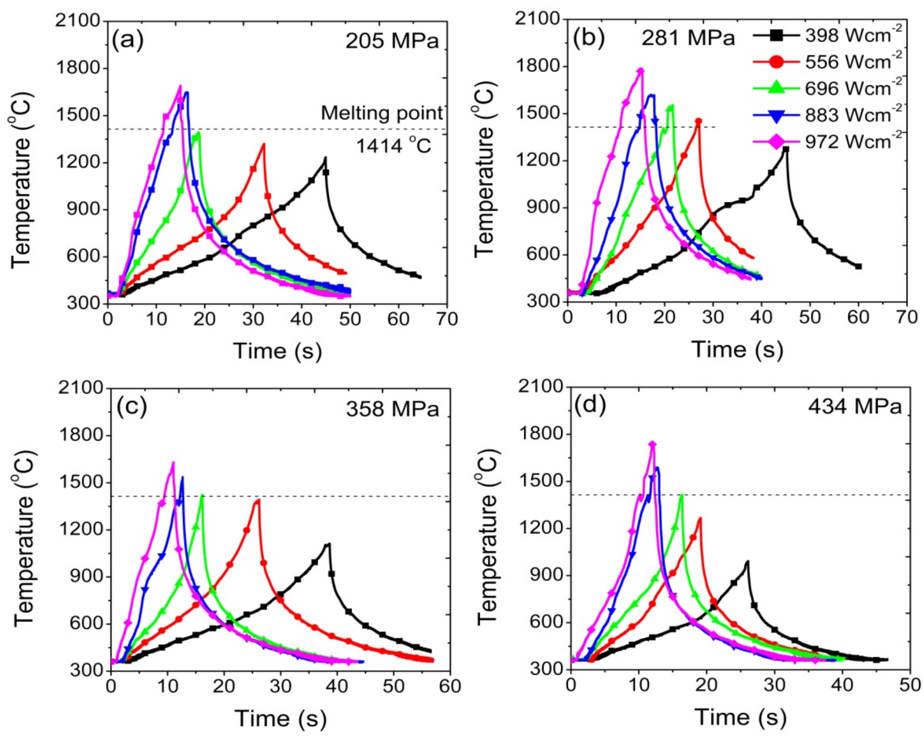

Figure 2. Temperature evolution during the laser irradiation of tensile loaded 304L stainless steel specimens for various laser power densities and tensile preload values. (**a**) 205 MPa, (**b**) 281 MPa, (**c**) 358 MPa and (**d**) 434 MPa.

With the increase of laser power density or preload, no significant variation trend in temperature profiles was observed. In general, temperature profiles are characterized by a plateau and a peak. The plateau appears at a temperature in the melting point range of 304L stainless steel (1414 °C–1496 °C), which indicates the melting of the specimen.

The plateau (solid-liquid platform) in the temperature profile appears due to the latent heat and belongs to the maximum detection limit of the pyrometer corresponding to melting depth. The peak corresponding to maximum value of temperature in the temperature profiles represents the failure temperature at which material get fractured and laser power turned off.

A comparison of temperature profiles in Figure 2a reveals the sharpness in initial temperature increase and an increase in the peak value with the increase of laser power density. This information illustrates the increased heating rate, the enhanced coupling of energy to the sample surface, and thicker molten layers with the increase of laser power density. The molten layer becomes transparent to laser energy relatively more quickly with the increase of laser power density; this is the cause of the small melting durations and quick recoveries and increases in temperature. With the increase of preload value from 205 MPa to 434 MPa in Figure 2a–d, no distinct difference in the trend of temperature variation is found. The only observed difference is the increased heating rate and different peak temperatures with the increase of preload values.

3.2. Stress Relaxation Behavior

Stress relaxation behavior for all the specimens fractured at four different preloading conditions under the increasing laser power density of continuous wave laser irradiations is presented in Figure 3.

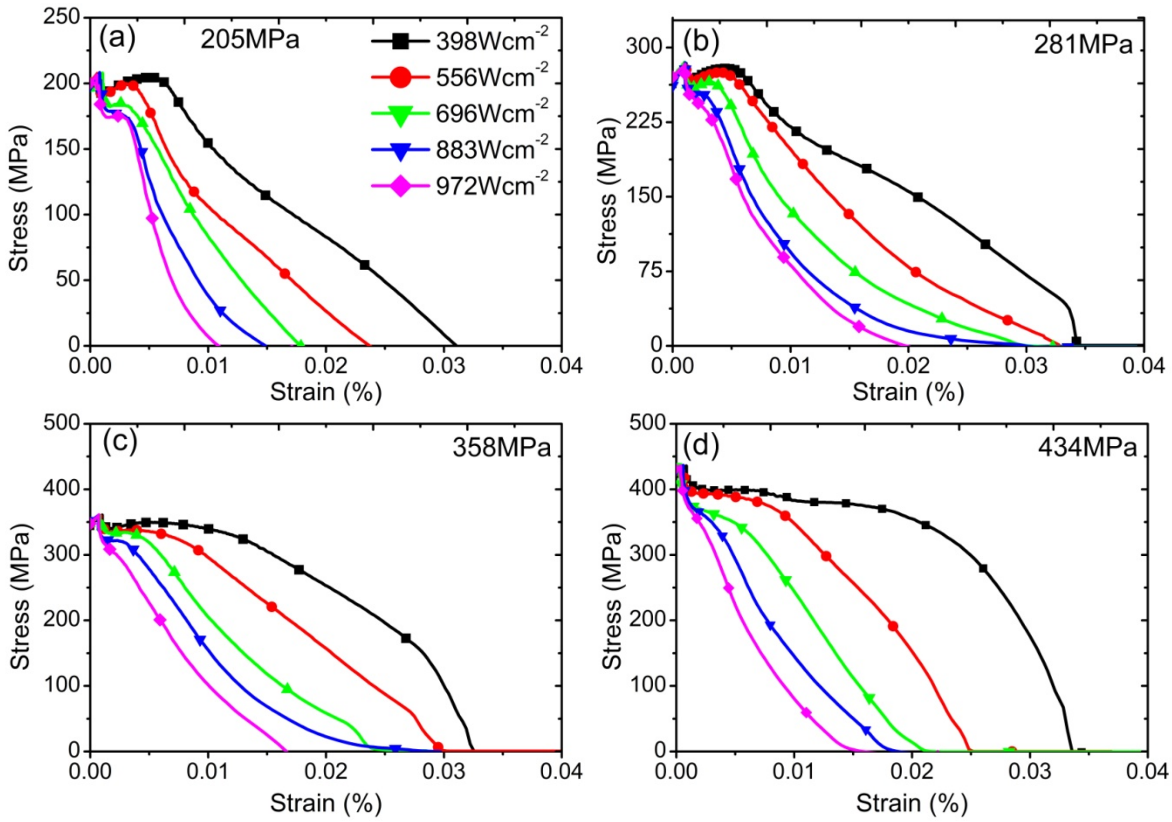

Figure 3. Stress relaxation characteristics of 304L stainless steel specimens deformed under different laser power densities and preloading levels: (**a**) 205 MPa, (**b**) 281 MPa, (**c**) 358 MPa and (**d**) 434 MPa.

The stress is determined by dividing the applied force by the initial gauge section. The strain is calculated by dividing the relative displacement (produced during the tensile test) of the specimen interfaces by the initial gauge length. In Figure 3a, for the lower laser power densities up to 556 $W \cdot cm^{-2}$, initially, flow stress decreased with the temperature increase. After a certain elevated temperature, flow stress increased significantly. The increase in flow stress indicates a strain hardening phenomenon at a certain temperature regime. Strain hardening arises due to microstructure changes induced by adiabatic heating and dynamic recovery processes [18–20].

With the increase of laser power density, the flow stress decreased considerably and sharply, with relatively reduced strain hardening effects. This shows that a rapid softening process occurs in high-temperature regimes, since the modulus and yield stress of materials generally decrease with an increase of temperature. Material strength degrades and materials ultimately undergo phase change effects like melting as the temperature continue to increase. As a result of these dynamic processes, the specimen loses mass, and its capacity to sustain mechanical load degrades [21]. A comparison of Figure 3a–d revealed that, with an increase of preload level, the flow curves turned to a relatively flat shape, with decreased final developed strain levels. The slight flatness of the flow curve with the increased preload level is an indication of limited brittle fracture behavior. In addition, the degree of strain hardening reduced for higher preloaded stress due to increased heating and softening rates.

Stress relaxation characteristics in Figure 3 indicate the sensitivity of the mechanical properties of 304L stainless steel to temperature. It can be seen that under the current test conditions, the material flow stress decreases with increasing laser power density. Moreover, with the increase of laser power density and preload level, the decreasing rate of flow stress was found to become sharp. This can be described as follows: by the increase of laser power density and temperature, the density and multiplication rate of structural defects decreased, resulting in a significant loss of resistance to plastic flow. Consequently, the 304L stainless steel specimen becomes softer and more ductile with an increase in laser power density or preload level. When a material is subjected to continually increasing temperature/laser power density and tensile preloading conditions, in general, its flow behavior (stress-strain) may be predominated by two competitive processes, i.e., work hardening rate and thermal softening rate. High rate deformation can induce the enhancement of the material's strength due to the high rate of strain/work hardening. On the other hand, an increase of temperature can cause a rapid reduction in the work hardening rate. In the present situation, after a sufficiently-elevated temperature is reached, thermal softening occurs dominantly, and the plastic flow is influenced mainly by the elevated temperature that eventually causes a rapid drop in the sustained load level and flow stress.

3.3. Strength Degradation

Figure 4a–d represents the 304L stainless steel specimen's strength degradation behavior as a function of laser power density under the fixed pre-loading. In Figure 4a, under the lowest laser power density of 398 $W \cdot cm^{-2}$ condition, the specimen's flow stress initially remained almost unchanged for a considerable period after being subjected to laser irradiation. Later, strain hardening effect was observed. Strain hardening corresponds to temperature-dependent strain localization within a specific range of strain and strain rate. In general, strain hardening is thought to be the result of carbon atoms diffusing around dislocation cores, and stopping them from progressing further [22]. Upon reaching a sufficiently-elevated temperature, the sustained load drops sharply, up to complete specimen failure.

For higher laser power densities, the time required for an initial drop in sustained load and the overall fracture process was shortened, with a sharp drop in the specimen's eventual degradation. As the laser power density increased, the specimen's temperature rose, which accelerates the thermal activation process and escalates the softening mechanism. The elevated temperature offers higher mobility to dynamically re-crystallized grains and defects annihilation, which in turn reduces the flow stress level. However, the overall decrease was relatively small for a low laser power density (398 W·cm^{-2}).

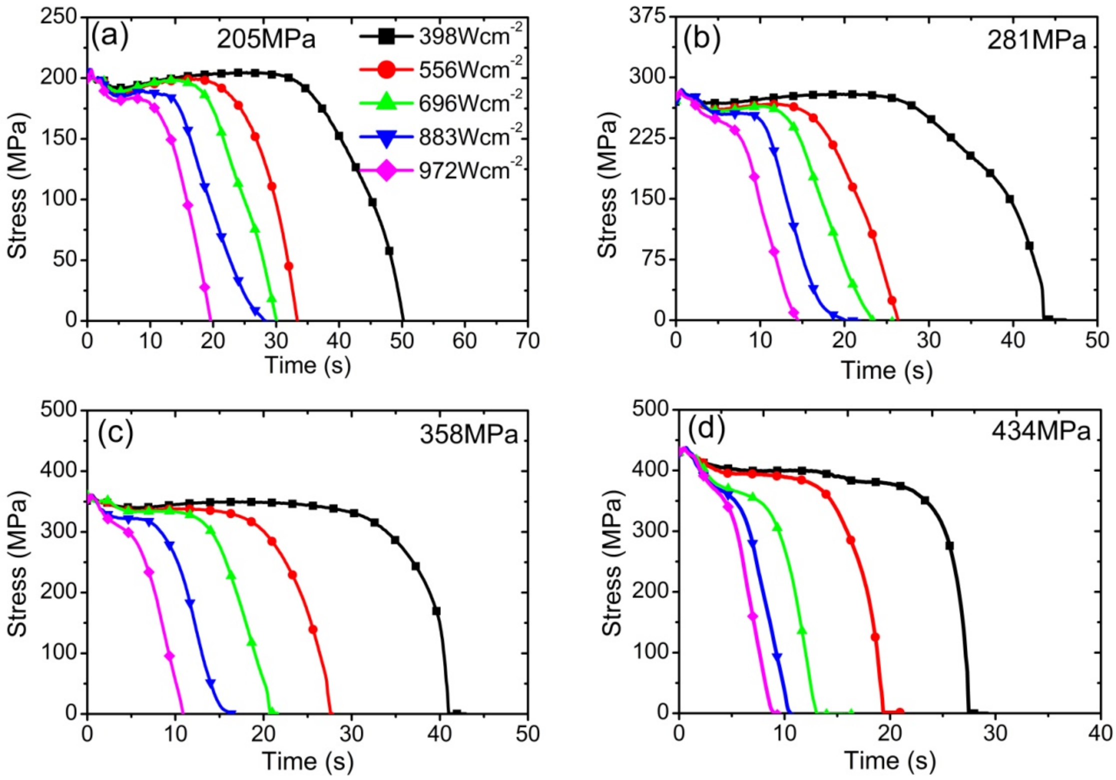

Figure 4. Strength degradation of 304L stainless steel specimens deformed under different laser power densities and preloading levels: (**a**) 205 MPa, (**b**) 281 MPa, (**c**) 358 MPa and (**d**) 434 MPa.

In Figure 4b–d, under the increased pre-loading states of 281 MPa, 358 MPa, and 434 MPa tensile loads, a similar pattern in the drop of the load bearing capability of 304L stainless steel specimens with an increase in laser power density is observed. Under the condition of lowest employed laser power density (398 W·cm^{-2}) in the Figure 2b–d, with an increase of preload level, a comparatively less delayed decrease of flow stress over a considerable range of plastic deformation is observed. After attaining a sufficiently-high temperature, the load sustained by the specimen started to drop, and fracture occurred abruptly. The mechanism for the primarily slow strength degradation is the low sensitivity of strengthening species in 304L stainless steel to modest temperature increases. Later, with the further increase in temperature, the strengthening species start to lose coherency, and favor mechanical degradation [23–26]. When the continually-heated specimen with limited thermally activated dynamics continually attains strain energy from the preload, it eventually becomes energetically supportive, to relieve the load through fractures in the specimen. With an increase in laser power densities, the specimen's failure arises in a similar pattern, and a comparatively sharp reduction of flow stress can be seen for all the preloaded levels. The specimen strength degradation and ultimate fracture are followed by two processes, namely, material loss from surface (recession/melting) and drop of yield strength with in-depth temperature increase.

3.4. Failure Time

Figure 5a,b demonstrate the failure time (the time from the start of laser irradiation to the failure/fracture of the specimen) as a function of laser power density and preloaded values respectively. The failure time depends on temperature, as well as on the temperature increase rate. The failure temperature belongs to the preloading value, while the temperature increase rate depends on laser power density. The temperature in the laser-focused area increases due to absorption of laser energy, which induces a decrease in specimen's strength, thermal expansion, and local combustion or melting. Consequently, the collective effect of mechanical stress and thermal effect gradually induce cracks and expansions, and reduce the specimen's failure time [13].

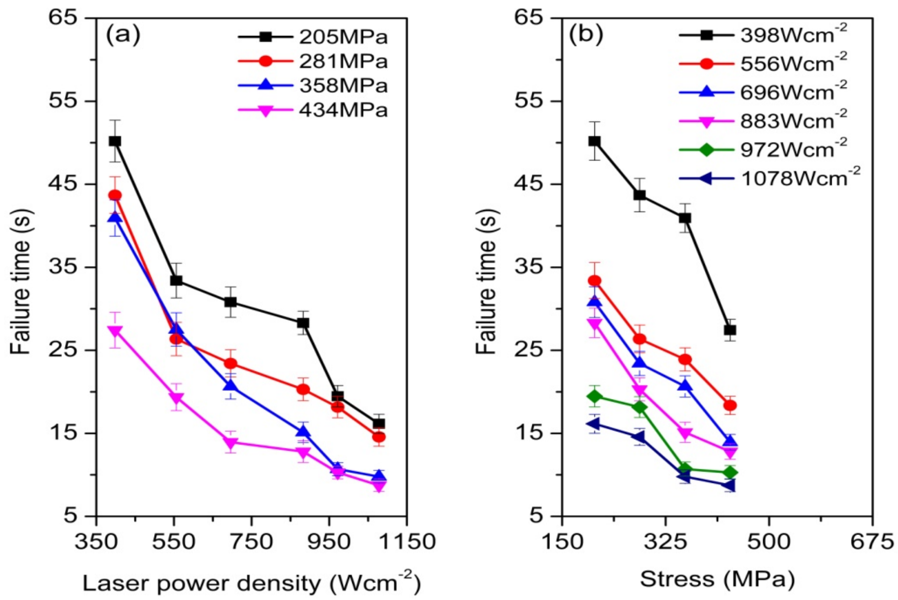

Figure 5. Failure time variation of 304L stainless steel specimens against (**a**) laser power density and (**b**) tensile load for varying experimental conditions.

From Figure 5, an overall decrease in failure time with the increase of laser power density or preload level is noticed. In Figure 5a, under the lowest applied preloading state of 205 MPa, a remarkable reduction in the failure time with an increase of laser power density is found. In contrast, for higher preloading states, a significant difference in failure time under lower laser power densities is found. In addition, for the higher pre-loading states, especially for 434 MPa, the increased laser power density has a relatively less pronounced effect on failure time. In brief, when the laser power density increases from 398 to 1078 W·cm^{-2}, the failure time decreases by 34 s, 29 s, 31 s, and 18.7 s, respectively, corresponding to preloaded states of 205 MPa, 281 MPa, 358 MPa, and 434 MPa. This indicates that for higher preloaded states, there is a relatively smaller impact of laser power density on failure time.

In Figure 5b, under the lowest laser power density of 398 W·cm^{-2}, a remarkable reduction in failure time with an increase of preload value is noted, whereas for higher laser power densities, relatively imperceptible effects of preloading values on failure time are found. When the preload level increased from 205 MPa to 434 MPa, the failure time decreased by 22.7 s, 15 s, 16.9 s 15.5 s, 9 s, and 7.4 s respectively, corresponding to laser power densities of 398 W·cm^{-2}, 556 W·cm^{-2}, 696 W·cm^{-2}, 883 W·cm^{-2}, 972 W·cm^{-2} and 1078 W·cm^{-2}. From these statistics, it may be said that for higher laser power densities, the preloading effects on the fracture of specimens becomes relatively less significant.

3.5. Fractographic Analysis

It is believed that, when subjected to thermo-mechanical loading, the change in the mechanical properties of the material is closely linked to the material's microstructure and its variations. In order to make clear the mechanisms of the effect of thermo-mechanical loading on the mechanical properties of 304L stainless steel, the fractographs of the deformed material were explored with scanning electron microscopy (SEM, FEI Quanta 250F, Thermo Fisher Scientific, Hillsboro, OR, USA).

Figure 6a–c represents the metallographs of 304L stainless steel fractured sections for specimens subjected to 205 MPa preloading state and irradiated by 398 W·cm^{-2}, 696 W·cm^{-2}, and 972 W·cm^{-2}

respectively. Primarily dimple-like morphology of the fractured surface indicates that the ductile failure mode is dominant for the 304L stainless steel for all laser power density conditions. Dimples are commonly assumed to be an indication of ductile fracture mode [27,28]. Additionally, voids, clusters with multiple voids, and tear edges/ridges can be seen. It is worth noting that with the increase of laser power density, dimple rupturing is the predominant failure mode. The fracture evolution process followed the void nucleation, growth, and coalescence. Ductile fractures (dimple formation) involve local plastic strain during the growth and coalescence of microvoids [29–31]. The higher strain concentrations favor local voids and crack growth around broken species [25,32]. At lower laser power densities, local stress and strain concentrations, and hence precipitate cracking tendency, are low, and the fracture process is less sensitive, with a limited number of voids and crack formations, while at higher power densities, increased temperatures and short range thermal stresses lead to tearing of dimples and the expansion of voids into cracks. The relatively increased density of dimples and voids with reduced sizes at higher laser power densities indicate large deformations before fracture.

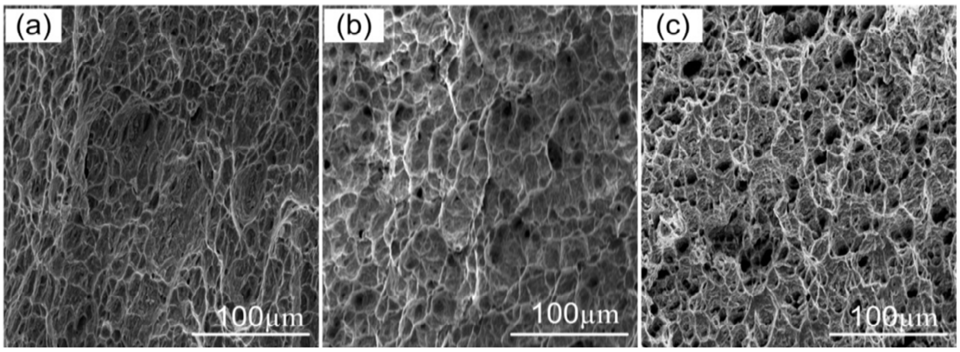

Figure 6. SEM images revealing the fracture morphology of 304L stainless steel specimen deformed under the condition of 205 MPa preload and for different laser power densities of (**a**) 398 W·cm^{-2}, (**b**) 696 W·cm^{-2} and (**c**) 972 W·cm^{-2} respectively.

The fracture morphology images in Figure 7a–c corresponding to 281 MPa preload and irradiated by 398 W·cm^{-2}, 696 W·cm^{-2}, and 972 W·cm^{-2} respectively reveal almost the same fracture mechanisms as those for 205 MPa preloading condition. An additional interesting observation in Figure 7a–c is the appearance of multiple voids on the fractured surfaces. In the early deformation stage, cracks arise in a localized region. As deformation continues, the cracks at the localized area merged, to form tearing along the edges and voids.

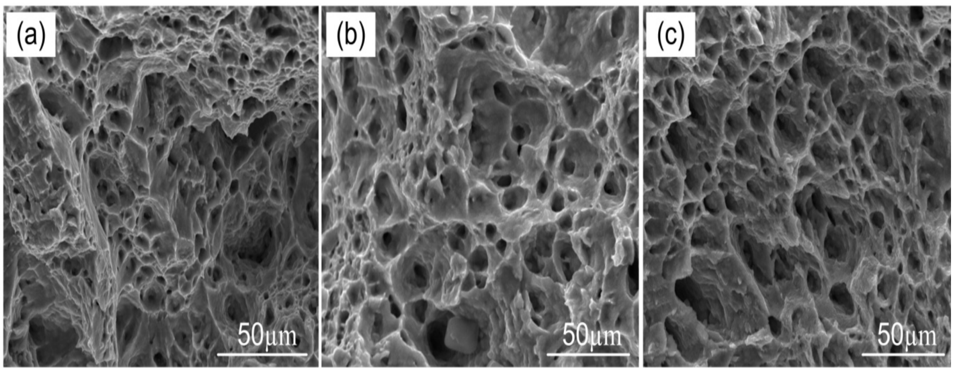

Figure 7. SEM images revealing the fracture morphology of 304L stainless steel specimen deformed under the condition of 281 MPa preload and for different laser power densities of (**a**) 398 W·cm^{-2}, (**b**) 696 W·cm^{-2} and (**c**) 972 W·cm^{-2} respectively.

The development of voids is the characteristic of large deformation within the primary grain boundary. Moreover, at higher power densities, the cracks initiated in the localized region merged into each other while creating the voids of increased size [33].

In Figure 8, with a further increase of preload level to 358 MPa, fracture characterizing features are similar to those of lower preload values. Again, void growth, nucleation, and coalescence is the governing mechanism. However, in Figure 9, for the highest employed preload value of 434 MPa, more distinct features, including cavities, isotropic thinner walls, and vein-like patterns are evident.

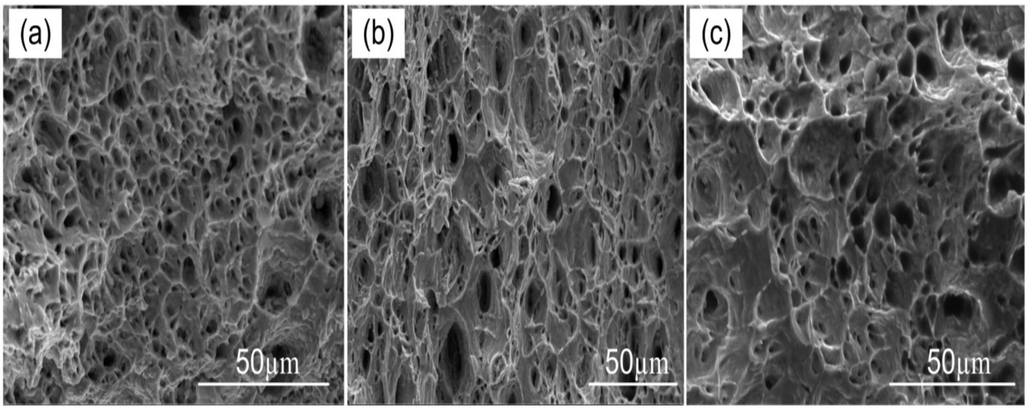

Figure 8. SEM images revealing the fracture morphology of 304L stainless steel specimen deformed under the condition of 358 MPa preload, and for different laser power densities: (**a**) 398 $W \cdot cm^{-2}$, (**b**) 696 $W \cdot cm^{-2}$ and (**c**) 972 $W \cdot cm^{-2}$ respectively.

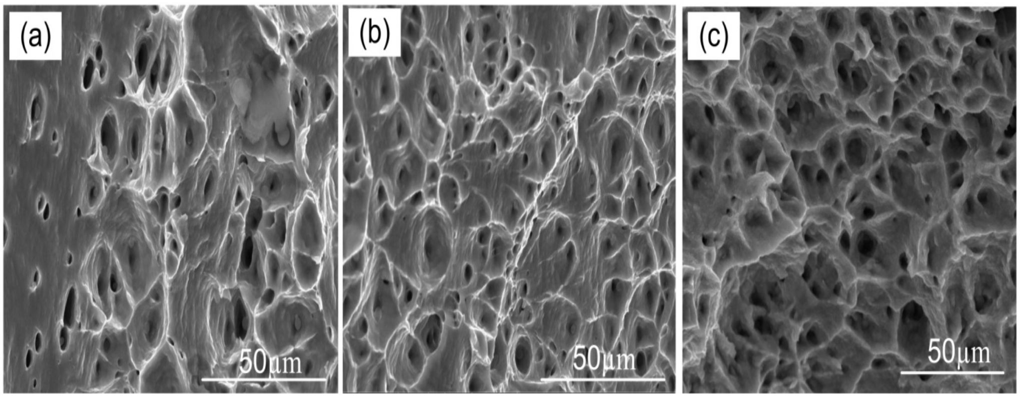

Figure 9. SEM images revealing the fracture morphology of 304L stainless steel specimen deformed under the condition of 434 MPa preload, and for different laser power densities: (**a**) 398 $W \cdot cm^{-2}$, (**b**) 696 $W \cdot cm^{-2}$ and (**c**) 972 $W \cdot cm^{-2}$ respectively.

With the increase of laser power density, the average spacing between the walls and veins reduced, which indicates a reduction in toughness and material strength compared to lower laser power densities. The formation of such features has been attributed to local softening or reduced viscosity within the shear bands [34,35]. Shear-induced structural disordering of the localized volume due to applied load or stress takes place on the shear plane [25,36]. In addition, temperature increase also leads to softening of the material on the shear plane. This softening leads to fast initiation and propagation of cracks, generating vein-like patterns on the fractured surface of the specimen. With the increase of laser power density, multiple cavitation events or nucleation of cavities and later growth and coalescence of these cavities through localization of veins occurred.

A comparison of fractographs corresponding to different preloading states reveals that fracture-characterizing features for 304L stainless steel mainly comprise micro-void nucleation, growth, and coalescence. Most of the fracture surfaces exhibited dimples and voids, which are indicative of ductile rupture. With the increase of laser power density, dimples rupture (density and of the voids/cracks increased) is the predominant fracture mode, while with an increase of preloading value, relatively more in-depth and severe deformation effects were observed.

4. Conclusions

An experimental study has been completed to investigate the deformation and fracture characteristics of 304L stainless steel under the simultaneous action of intense laser heating and mechanical loading. Although the deformation experiments were performed at a variety of load levels, significantly more pronounced influence of laser power density/temperature on specimen strength degradation was reported. This indicates the high sensitivity of mechanical behavior of 304L stainless steel to elevated temperatures. The stress-strain curves indicated that the specimens experienced slight strain hardening in certain temperature ranges prior to fracture. The specimen's ultimate failure time was found to be reduced by increasing either the laser power density or preload level. Fracture analysis revealed the overall ductile fracture mode characterized by microvoids and dimple structures. With the increase of laser power density, dimple ruptures are the primary fracture mode, while with an increase in preload value, relatively more in-depth and severe deformation effects were observed. The reasons and characterization of 304L stainless steel failure under the simultaneous action of laser heating and tensile stress have been presented in detail.

Author Contributions: Conceptualization, M.J. and Z.S.; Methodology, Z.L. and M.J.; Formal Analysis, M.J. and Z.L.; Investigation, M.J.; Writing-Original Draft Preparation, M.J.; Writing-Review & Editing, N.U.H. and M.S.; Supervision, Z.S.

Funding: This research was funded by National Natural Science Foundation of China grant number [61605079] and Fundamental Research Funds for the Central Universities grant number [30916014112-020].

Conflicts of Interest: The authors declare no conflict of interest. The funders had no role in the design of the study; in the collection, analyses, or interpretation of data; in the writing of the manuscript, and in the decision to publish the results.

References

1. Lee, W.-S.; Lin, C.-F. Impact properties and microstructure evolution of 304L stainless steel. *Mater. Sci. Eng. A* **2001**, *308*, 124–135. [CrossRef]
2. Chen, J.; Young, B. Stress–strain curves for stainless steel at elevated temperatures. *Eng. Struct.* **2006**, *28*, 229–239. [CrossRef]
3. Faggiano, B.; Matteis, G.D.; Landolfo, R.; Mazzolani, F.M. Behaviour of aluminium alloy structures under fire. *J. Civ. Eng. Manag.* **2004**, *10*, 183–190. [CrossRef]
4. Medford, J.E.; Gray, P.M. The response of structural materials to combined laser and mechanical loading. In *15th Thermophysics Conference*; AIAA: Snowmass, CO, USA, 1980; p. 1550.
5. Shanmugam, N.S.; Buvanashekaran, G.; Sankaranarayanasamy, K.; Manonmani, K. Some studies on temperature profiles in AISI 304 stainless steel sheet during laser beam welding using FE simulation. *Int. J. Adv. Manuf. Technol.* **2009**, *43*, 78–94. [CrossRef]
6. Semb, E. Behavior of Aluminum at Elevated Strain Rates and Temperatures. Master's Thesis, Institutt for konstruksjonsteknikk, Trondheim, Norway, 14 June 2013.
7. Griffis, C.; Chang, C.; Stonesifer, F. Thermo-mechanical response of tension panels under intense rapid heating. *Theor. Appl. Fract. Mech.* **1985**, *3*, 41–48. [CrossRef]
8. Jelani, M.; Li, Z.; Shen, Z.; Sardar, M.; Tabassum, A. Experimental investigations on thermo mechanical behaviour of aluminium alloys subjected to tensile loading and laser irradiation. In Proceedings of the 4th International Symposium on Laser Interaction with Matter, Chengdu, China, 6–9 November 2016; SPIE: Bellingham, WA, USA, 2017.
9. Sierakowski, R.L. Strain rate behavior of metals and composites. In Proceedings of the Convegno IGF XIII Cassino 1997, Cassino, Italy, 27–28 May 1997.

10. El-Magd, E.; Abouridouane, M. Characterization, modelling and simulation of deformation and fracture behaviour of the light-weight wrought alloys under high strain rate loading. *Intern. J. Impact Eng.* **2006**, *32*, 741–758. [CrossRef]
11. Lee, W.S.; Sue, W.C.; Lin, C.F.; Wu, C.J. The strain rate and temperature dependence of the dynamic impact properties of 7075 aluminum alloy. *J. Mater. Process. Technol.* **2000**, *100*, 116–122. [CrossRef]
12. Zhu, Y.; Ye, X.; Lin, X.; Wei, C.; Wang, L.; Cheng, D. Experimental investigation on the damage effect of steel structure by continuous laser under preloaded invariable stretching stress. In Proceedings of the 2nd International Symposium on Laser Interaction with Matter, Xi'an, China, 9–12 September 2012; SPIE: Bellingham, WA, USA, 2013.
13. Long, L.C.; Wang, T.T.; Liu, L.T. Tensile and compression test of carbon/epoxy composite laminate under combined action of laser irradiation and load. *Mater. Res. Innov.* **2015**, *19*, 171–176. [CrossRef]
14. Chang, C.; Griffis, C.; Stonesifer, F.; Nemes, J. Thermomechanical effects of intense thermal heating on materials/structures. *J. Thermophys. Heat Transf.* **1987**, *1*, 175–181. [CrossRef]
15. Mousavi, S.A.; Miresmaeili, R. Experimental and numerical analyses of residual stress distributions in tig welding process for 304l stainless steel. *J. Mater. Process. Technol.* **2008**, *208*, 383–394. [CrossRef]
16. Rai, R.; Elmer, J.; Palmer, T.; DebRoy, T. Heat transfer and fluid flow during keyhole mode laser welding of tantalum, Ti–6Al–4V, 304L stainless steel and vanadium. *J. Phys. D Appl. Phys.* **2007**, *40*, 5753. [CrossRef]
17. Jelani, Z.; Li, Z.; Shen, Z.; Sardar, M. Thermomechanical response of aluminum alloys under the combined action of tensile loading and laser irradiations. *Chin. Phys. B* **2018**, *27*, 037901. [CrossRef]
18. Stout, M.; Follansbee, P. Strain rate sensitivity, strain hardening, and yield behavior of 304l stainless steel. *J. Eng. Mater. Technol.* **1986**, *108*, 344–353. [CrossRef]
19. De, A.K.; Speer, J.G.; Matlock, D.K.; Murdock, D.C.; Mataya, M.C.; Comstock, R.J. Deformation-induced phase transformation and strain hardening in type 304 austenitic stainless steel. *Metall. Mater. Trans. A* **2006**, *37*, 1875–1886. [CrossRef]
20. McQueen, H.; Jonas, J. Recovery and recrystallization during high temperature deformation. In *Treatise on Materials Science & technology*; Elsevier: New York, NY, USA, 1975; Volume 6, pp. 393–493.
21. Legner, H.; Popper, L.; Laughlin, W.; Pugh, E. Analysis of rp laser experiments on tensile-loaded materials. In Proceedings of the 24th Plasma Dynamics and Lasers Conference, Orlando, FL, USA, 6–9 July 1993; AIAA: Reston, VA, USA, 1993.
22. Cornet, C.; Wackermann, K.; Stöcker, C.; Christ, H.; Lupton, C.; Hardy, M.; Tong, J. Effects of temperature and hold time on dynamic strain aging in a nickel based superalloy. *Mater. High Temp.* **2014**, *31*, 226–232. [CrossRef]
23. Florando, J.; Margraf, J.; Reus, J.; Anderson, A.; McCallen, R.; LeBlanc, M.; Stanley, J.; Rubenchik, A.; Wu, S.; Lowdermilk, W. Modeling the effect of laser heating on the strength and failure of 7075-T6 aluminum. *Mater. Sci. Eng. A* **2015**, *640*, 402–407. [CrossRef]
24. Jelani, M.; Li, Z.; Shen, Z.; Sardar, M. Failure response of simultaneously pre-stressed and laser irradiated aluminum alloys. *Appl. Sci.* **2017**, *7*, 464. [CrossRef]
25. Maleque, M.A.; Salit, M.S. Mechanical failure of materials. In *Materials Selection and Design*; Springer: Berlin, Germany, 2013; pp. 17–38.
26. Santos, J.L.d.; Monteiro, S.N.; Cândido, V.S.; Silva, A.O.d.; Tommasini, F.J. Fracture modes of aisi type 302 stainless steel under metastable plastic deformation. *Mater. Res.* **2017**, 596–602. [CrossRef]
27. Srivatsan, T.S.; Sriram, S.; Veeraraghavan, D.; Vasudevan, V. Microstructure, tensile deformation and fracture behaviour of aluminium alloy 7055. *J. Mater. Sci.* **1997**, *32*, 2883–2894. [CrossRef]
28. Wojtaszek, M.; Sleboda, T.; Czulak, A.; Weber, G.; Hufenbach, W. Quasi-static and dynamic tensile properties of ti-6al-4v alloy. *Arch. Metall. Mater.* **2013**, *58*, 1261–1265. [CrossRef]
29. Wang, P.; Lu, S.; Xiao, N.; Li, D.; Li, Y. Effect of delta ferrite on impact properties of low carbon 13Cr-4Ni martensitic stainless steel. *Mater. Sci. Eng. A* **2010**, *527*, 3210–3216. [CrossRef]
30. Hassan, S.F.; Zabiullah, S.; Al-Aqeeli, N.; Gupta, M. Magnesium nanocomposite: Effect of melt dispersion of different oxides nano particles. *J. Mater. Res.* **2016**, *31*, 100–108. [CrossRef]
31. Dieter, G.E.; Bacon, D.J. *Mechanical Metallurgy*; McGraw-hill: New York, NY, USA, 1986; Volume 3.
32. Xue, Y.; McDowell, D.; Horstemeyer, M.; Dale, M.; Jordon, J. Microstructure-based multistage fatigue modeling of aluminum alloy 7075-t651. *Eng. Fract. Mech.* **2007**, *74*, 2810–2823. [CrossRef]

33. Feng, Y.; Zhang, W.; Zeng, L.; Cui, G.; Chen, W. Room-temperature and high-temperature tensile mechanical properties of TA15 titanium alloy and TiB whisker-reinforced TA15 matrix composites fabricated by vacuum hot-pressing sintering. *Materials* **2017**, *10*, 424. [CrossRef] [PubMed]
34. Talonen, J.; Hänninen, H. Formation of shear bands and strain-induced martensite during plastic deformation of metastable austenitic stainless steels. *Acta Mater.* **2007**, *55*, 6108–6118. [CrossRef]
35. Hamada, A.; Karjalainen, L.; Misra, R.; Talonen, J. Contribution of deformation mechanisms to strength and ductility in two Cr–Mn grade austenitic stainless steels. *Mater. Sci. Eng. A* **2013**, *559*, 336–344. [CrossRef]
36. Sun, B.; Tan, J.; Pauly, S.; Kühn, U.; Eckert, J. Stable fracture of a malleable Zr-based bulk metallic glass. *J. Appl. Phys.* **2012**, *112*, 103533. [CrossRef]